atmosphere

MDPI

Article

Impacts of the Interannual Variability of the Kuroshio Extension on the East Asian Trough in Winter

Jianxiang Sun [1,2], Suping Zhang [3,*], Yuxi Jiang [4], Yanshuo Wang [3], Baoqin Wu [5] and Haijiao Wang [6]

1 Tianjin Navigation Instrument Research Institute, Tianjin 300131, China; sunjxouc@163.com
2 Laboratory of Science and Technology on Marine Navigation and Control, China State Shipbuilding Corporation, Tianjin 300131, China
3 Physical Oceanography Laboratory, Ocean University of China and Qingdao National Laboratory for Marine Science and Technology, Qingdao 266100, China; wangyanshuo@stu.ouc.edu.cn
4 National Marine Data and Information Service, Tianjin 300171, China; jiang.meteorol@gmail.com
5 Naval Institute of Hydro Graphic Surveying and Charting, Tianjin 300171, China; 13512068930@163.com
6 GUANGXI YI FU Engineering Consulting Limited, Tianjin 300171, China; 15101521050@163.com
* Correspondence: zsping@ouc.edu.cn

Abstract: The responses of the East Asian Trough (EAT) to the Kuroshio Extension (KE) interannual fluctuation and the underlying mechanisms in the boreal winter are investigated through the lag regression approach in this study. When the KE is in the stable state, the sea surface temperature (SST) front is strengthened, with cold (warm) SST anomaly in the western (eastern) region of the KE, releasing less (more) heat into the atmosphere. The opposite patterns hold for the KE unstable periods. The analysis of the observations shows that the stable KE corresponds to a deeper EAT, accompanied with a stronger winter monsoon over Mongolia and northeastern China. The atmospheric Rossby waves, transient eddies, and thermal winds are found to be responsible for this relationship between the KE and EAT. The SST warming in the lower reaches of the KE excites the Rossby wave activity that propagates toward East Asia, leading to 25% of the EAT amplification. Meanwhile, influenced by the KE-induced Rossby waves, the background baroclinicity is intensified over Japan, which enhances the transient eddy activity, contributing to another 42% magnitude of the EAT deepening. In addition, as depicted by the thermal wind theory, the strong SST cooling in the upper branch of the KE forces an anomalous cyclonic circulation through modifying the meridional temperature gradient, facilitating the EAT development. The finding points to the better understandings of the EAT and associated East Asian winter climate variability, which are crucial for their major economic and social impacts on the large populations in the region.

Keywords: Kuroshio Extension stability; East Asian trough; atmospheric circulation; eddy-mean flow interaction

check for updates

Citation: Sun, J.; Zhang, S.; Jiang, Y.; Wang, Y.; Wu, B.; Wang, H. Impacts of the Interannual Variability of the Kuroshio Extension on the East Asian Trough in Winter. *Atmosphere* **2022**, *13*, 996. https://doi.org/10.3390/atmos13070996

Academic Editor: Yoshihiro Tomikawa

Received: 26 May 2022
Accepted: 16 June 2022
Published: 21 June 2022

Publisher's Note: MDPI stays neutral with regard to jurisdictional claims in published maps and institutional affiliations.

Copyright: © 2022 by the authors. Licensee MDPI, Basel, Switzerland. This article is an open access article distributed under the terms and conditions of the Creative Commons Attribution (CC BY) license (https://creativecommons.org/licenses/by/4.0/).

1. Introduction

The East Asian trough (EAT), as one of the three major troughs in the winter of the Northern Hemisphere, is featured by the strongest negative deviation from the zonal mean over East Asia [1,2]. Its formation is mainly attributed to the large-scale thermal contrast between the cold Eurasian continent and warm Pacific Ocean [3,4]. As an important climate system, the EAT is crucial for the winter climate in the North Pacific and East Asia. To the east of the EAT, the EAT sustains a sharp meridional temperature gradient by bringing the cold monsoonal air to the warm ocean, which is critical for the North Pacific storm track [5–7]. Over the upstream side of the EAT, the East Asian winter monsoon (EAWM), highly associated with the EAT system, dominants the winter climate of the East Asian countries. Strong EAWM related with the deep EAT often brings cold surges and blizzard to East Asia, resulting in substantial economic and social losses [8,9]. Therefore, it is of

great importance to understand the factors and processes of the EAT, which can help us to improve the forecasts of the EAT and its representation in climate model.

The variations of the EAT and associated EAWM could be influenced by many factors at different time scales. On the synoptic time scale, the upper-level short waves originate from Europe and propagate eastward over the Eurasian continent, resulting in the EAT's development and subsequent outbreaks of cold events [10]. On the intraseasonal time scale, the upper-tropospheric Rossby wave train and the Rossby wave-induced changes of the transient eddy activities can lead to the EAT's variation in intensification [11]. Many factors are found to have impacts on the EAT's strength on the annual time scale, such as the Arctic Oscillation (AO) [12], North Atlantic Oscillation (NAO) [13,14], autumn Eurasian snow cover [15], and autumn Arctic sea ice [16]. In addition, the decadal weakening of the EAT around the mid-1980s is largely attributed to the intense positive sea surface temperature (SST) anomalies over the North Pacific [17] and anthropogenic forcings from greenhouse gases and anthropogenic aerosols [18,19]. Few of the existing studies, however, dig deep into the potential role of the Kuroshio Extension (KE) on influencing the EAT, even though as the underlying surface of the EAT, the KE induces rich air–sea interactions through large surface heat fluxes [20–23].

The KE, known as the strongest western boundary current in the world, shows a bimodal interannual fluctuation between a stable state, with a sharp SST front and subdued ocean mesoscale eddy activity; and an unstable state, in which the SST front is weaker and accompanied with substantial eddies [24]. This KE fluctuation is found to have significant impacts on not only the local atmospheric boundary layer and clouds [25–28] and North Pacific storm track, but also the large-scale circulation, among which the eddy–mean flow interaction and Rossby wave activity are suggested to play crucial roles [29–34]. Ma et al. demonstrates that the unstable KE state generates the mesoscale SST variability, enhancing the winter cyclogenesis via moist baroclinic instability [29]. The modulation in the storm track in turn leads to a barotropic anticyclone anomaly over the Eastern Pacific through the eddy–mean flow interactions, strongly influencing the blocking frequency there [31]. On the other hand, in the stable phase of the KE, the SST warming in the Kuroshio-Oyashio Extension region leads to an upward surface heating and a northeastward shift of the storm track, exciting the Rossby wave that propagates poleward and eastward, resulting in an equivalent barotropic large-scale signal, with a downstream weakened surface Aleutian low and a low over the Arctic [32,33].

Compared to the well-known impacts of the KE fluctuation on the local and downstream atmosphere, there is a lack of understanding of the relationship between the KE and upstream EAT. In addition, although [31,32] did not probe deeper into the EAT responses to the KE variability, the geopotential height responses of their results over East Asia imply a possible interannual linkage between the EAT and KE, giving us an interest in exploring the relationship between them. Therefore, the objectives of this study are as follows: first, to assess and examine the link between the KE fluctuation and EAT at the interannual time scale; second, to investigate the underlying physical mechanisms. The data and methods used in the present study are described in Section 2. Section 3 shows the results. In Section 4, we summarize and discuss the results.

2. Data and Methodology

2.1. Data

The sea surface height anomaly (SSHA) from the Archiving, Validation and Interpretation of Satellite Oceanographic (AVISO), available in daily mean on a $0.25^\circ \times 0.25^\circ$ grid from January 1993 [35], is used in this study. The daily means of sensible and latent heat fluxes with a $1^\circ \times 1^\circ$ resolution are from the Objectively Analyzed Air–Sea Fluxes (OAFlux) provided by the Woods Hole Oceanographic Institution [36]. To obtain the anomalous atmospheric circulations, we analyzed the atmospheric variables, including geopotential height, air temperature, SST, snow cover, and zonal and meridional wind components, from the fifth major global ReAnalysis data by the European

Centre for Medium-Range Weather Forecasts (ERA5). This dataset has 31 km horizontal resolution and 137 levels in the vertical up to 0.01 hPa, with hourly intervals (https://www.ecmwf.int/en/newsletter/147/news/era5-reanalysis-production, accessed on 19 January 2022). The data used in this study are from the period of 1993-2019.

2.2. Methodology

Following [37], we characterized the interannual KE dynamical state using the KE index (KEI), which is valued as the region-mean 1-year lowpass filtered SSHA in 31–36° N, 140–165° E. The EAT intensity index (EATII), defined as the averaged z_{500} for the area between 125–145° E and 35–50° N, was used in this study.

Over midlatitudes, the anomalous processes were explained through the barotropic vorticity equation. The anomalous Rossby wave source (RWS) diagnostic equation, proposed by Sardeshmukh and Hoskins [38], was computed:

$$\mathrm{RWS}' = -\nabla\cdot\left(V'_\chi\overline{\xi}\right) - \nabla\cdot\left(\overline{V}_\chi\xi'\right). \tag{1}$$

Here, V_χ is the divergent winds calculated from the velocity potential, and ξ represents the absolute vorticity. The primes and overbars indicate the perturbations and winter mean-values, respectively.

To illustrate the propagation of Rossby waves associated with the KE fluctuation, the wave activity flux (WAF) paralleling to its local group velocity in a phase-independent manner on the zonally varying basic flow was employed [39,40]. The WAF is defined as follows:

$$\vec{W} = \frac{1}{2|\vec{U}|}\begin{pmatrix} u\left(\psi_x'^2 - \psi'\psi'_{xx}\right) + v\left(\psi'_x\psi'_y - \psi'\psi'_{xy}\right) \\ u\left(\psi'_x\psi'_y - \psi'\psi'_{xy}\right) + v\left(\psi_y'^2 - \psi'\psi'_{yy}\right) \\ \frac{f}{R\sigma/p}\left\{u\left(\psi'_x\psi'_p - \psi'\psi'_{xp}\right) + v\left(\psi'_y\psi'_p - \psi'\psi'_{yp}\right)\right\} \end{pmatrix} \tag{2}$$

where (u, v) is the climatological mean horizontal wind velocity averaged in the winter over the 1993–2018 period, $|\vec{U}|$ is the speed of the basic horizontal mean flow, ψ' is the perturbation geostrophic streamfunction, f is the Coriolis parameter, R is the gas constant, p is the pressure, and $\sigma = \left(R\overline{T}/C_p p\right) - d\overline{T}/dp$, where T is the temperature and C_p is the specific heat at a constant pressure. Subscripts x, y, and, p denote the partial derivatives in the zonal, meridional, and vertical directions, respectively. The wave disturbances are emitted (absorbed) where there is a divergence (convergence) of the WAF.

Following Hoskins and Valdes [41], the maximum Eady growth rate (EGR) at the 850-hPa level was calculated, which is used to estimate the baroclinicity changes associated with the shift of KE dynamical state. The formula is

$$\sigma = 0.31\frac{f}{N}\left|\frac{\partial U}{\partial z}\right| \tag{3}$$

where f is the Coriolis parameter, N is the Brunt-Väisälä frequency, U is the speed of horizontal winds, and z is the vertical height.

The storm-track was measured by the 300-hPa meridional wind variance $v'v'$, where the prime indicates that a 2.5–6-day bandpass 31-point filter [42] is applied to effectively extract the synoptic-scale transient eddies.

The eddy-induced geopotential height tendency defined by Lau and Nath is shown in Equation (4) [43]:

$$\left(\frac{\partial Z}{\partial t}\right)_{eddy} = \frac{f}{g}\nabla^{-2}\left[-\nabla\cdot\left(\overline{V\prime\zeta\prime}\right)\right] \tag{4}$$

where Z is the monthly mean geopotential height, g is the gravitational acceleration, V' and ζ' are the synoptic-scale daily winds and relative vorticity subject to a 2.5–6-day

bandpass filtering. The geopotential height tendency generated by the Rossby waves was also evaluated by applying the 8–90-day Butterworth bandpass.

To evaluate the influences of KE variability on the East Asian climate, the first law of thermodynamics was calculated:

$$\frac{\partial T}{\partial t} = -\vec{V}\cdot\nabla T - \omega\left(\frac{\partial T}{\partial p} - \frac{R}{C_p}\frac{T}{P}\right) + \frac{Q}{C_p\rho} \tag{5}$$

The local change in air temperature $\left(\frac{\partial T}{\partial t}\right)$ depends on the horizontal heat transport $(-\vec{V}\cdot\nabla T)$, vertical heat transport $\left(-\omega\left(\frac{\partial T}{\partial p} - \frac{R}{C_p}\frac{T}{P}\right)\right)$, and diabatic heating $\left(\frac{Q}{C_p\rho}\right)$. The diabatic heating term was computed as the residue from the other three known terms.

This study focused on the boreal winter consisting of 90 days from 1 December to 28 February (DJF). The winter of 1993 denotes the December 1993 and January, February 1994. All the data were linearly detrended to eliminate the climate trend before analysis (non-detrended analysis derives similar results). The significances of filed anomalies were estimated using Student's t test with effective degree of freedom proposed by [44], due to the non-negligible autocorrelation of KE index.

2.3. Estimating the Atmospheric Responses

Over midlatitudes, the atmospheric responses to the extratropical boundary forcing are overlapped by the atmospheric internal variability and tropical remote forcing (i.e., ENSO), which makes them difficult to access. To solve this problem, we followed the approach proposed by Révelard et al. [32], which assumes that an atmospheric variable $x(t)$ can be decomposed into the quasi-equilibrium atmosphere responses to the KE 2 months earlier and ENSO 1 month earlier, say, $\alpha KEI(t-2)$ and $\beta e(t-1)$, respectively, and the rapid atmospheric intrinsic variability, $n(t)$:

$$x(t) = \alpha KEI(t-2) + \beta e(t-1) + n(t) \tag{6}$$

with α and β being the response or feedback parameters, KEI being the KE index, and e being the ENSO signal (defined as the Niño 3.4 index by the average of SST anomalies over the region 5° N–5° S and 170°–120° W compared to 1981–2010). Recent studies proposed that it generally takes 2 months for the transient eddy–mean flow interactions to fully transform the initial extratropical SST anomalies-induced local baroclinic response into the large-scale equivalent barotropic one [32,45,46]. The imprints of KE on the large-scale atmosphere circulations are similar as the atmosphere lags the ocean for 1 to 6 months, but the responses are strongest with a delay of 2 months (not shown). Moreover, it takes 1 month for ENSO teleconnections to reach East Asia. Therefore, in this study, we consider it is appropriate to regard the atmosphere response times to the KE and ENSO as 2 months and 1 month, respectively.

To estimate α, the first necessary step to be carried out is to remove the ENSO signal. Here, we define the ENSO-filtered atmospheric variable and KEI as

$$\widetilde{x}(t) = x(t) - Ae(t-1) \tag{7}$$

$$\widetilde{KEI}(t) = KEI(t) - Be(t+1) \tag{8}$$

where $A = \langle x(t), e(t-1)\rangle / \langle e(t-1), e(t-1)\rangle$ and $B = \langle KEI(t), e(t+1)\rangle / \langle e(t+1), e(t+1)\rangle$, and $\langle p, q\rangle$ represents the covariance between p and q. Taking Equations (7) and (8) into Equation (6) and taking into account that the KE variability is not correlated with the atmospheric intrinsic variability leads to

$$\widetilde{x}(t) = \alpha\widetilde{KEI}(t-2) + n(t) \tag{9}$$

Multiplying $\widetilde{KEI}(t-2)$ on both sides of Equation (9) and then taking ensemble average, α can be expressed as

$$\alpha = \frac{\langle \widetilde{x}(t), \widetilde{KEI}(t-2) \rangle}{\langle \widetilde{KEI}(t-2), \widetilde{KEI}(t-2) \rangle} \tag{10}$$

This approach has been widely used, not only in accessing the local influences of SST on the overlying atmosphere [47], but also in estimating the atmospheric nonlocal responses to oceanic variability [32,48–50].

3. Results

3.1. The KE Index

As displayed in Figure 1a, the KE shows a bimodal interannual fluctuation between positive and negative phases. Here, since we focused on the atmospheric responses in DJF to the KE state 2 months earlier, when the mean KEI from October to December (OND) was larger than 0, we identified it as the KE stable period (SP), which was featured by the remarkable positive SSHA to the south of the KE axis around 35° N and weak negative SSHA to the north (Figure 1b), implying a steadier and stronger KE jet. The KE unstable period (USP) was chosen if the OND KEI was less than 0, bearing a basically opposite SSHA pattern to that in the SPs but with a smaller amplification (Figure 1c). The variation feature of the KE dynamical state and corresponding SSHA pattern are in agreement with Qiu et al. [37].

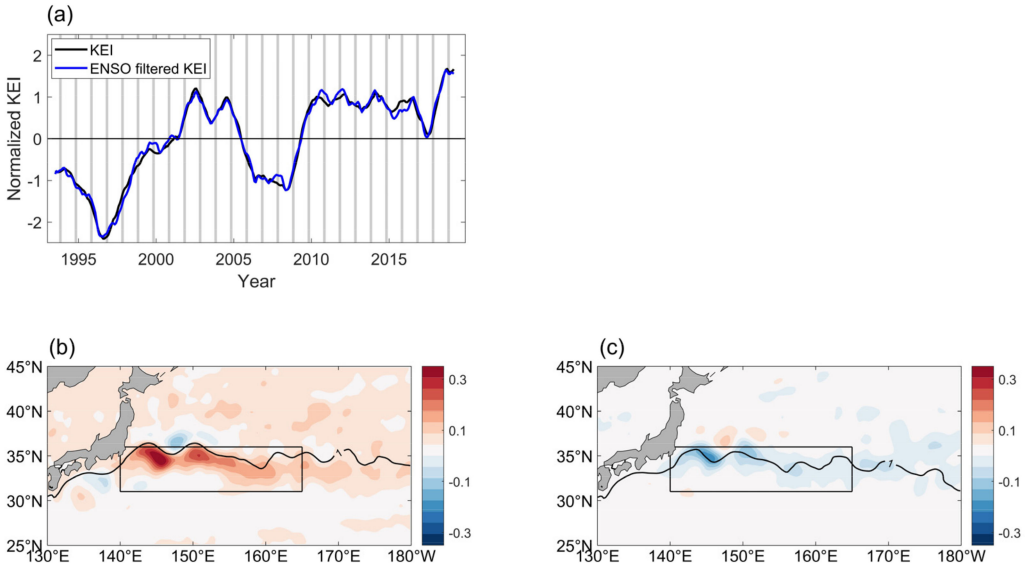


Figure 1. (**a**) Time series of the monthly normalized KEI (black line) and ENSO-filtered KEI (blue line) based on the AVISO SSHA observations. The KEI in OND is marked by grey bars. Composite SSHA (shading, unit: m) and KE axis defined by the 1 m sea surface height (black curve, unit: m) for the (**b**) SPs and (**c**) USPs from 1993 to 2018. The black rectangles in (**b**,**c**) denote the area used for calculating the KEI.

Figure 2 shows the estimated winter-mean response of SST to the KE variability, along with the relevant turbulent heat fluxes (THF) response. In the meridional direction, it was evident that there was a negative SST anomaly around the KE front, modifying the SST front. In the zonal direction, the SST decreased (increased) by 1 K (0.5 K) in the western (eastern) part of the KE region. The corresponding THF anomaly of -30 W m^{-2} (20 W m^{-2}), which amounts to about 10% of the winter background heat fluxes, is supposed to have significant influences on the atmosphere. Furthermore, it should be noted that the SST cooled down and THF increased in the East China Sea and Sea of Japan. This implies a stronger EAWM

and deeper EAT in the SPs, as the stronger cold air advection from the Eurasia continent can enhance the THF by increasing the temperature difference of the sea–air interface and thus cool down the SST, and vice versa for the USPs.

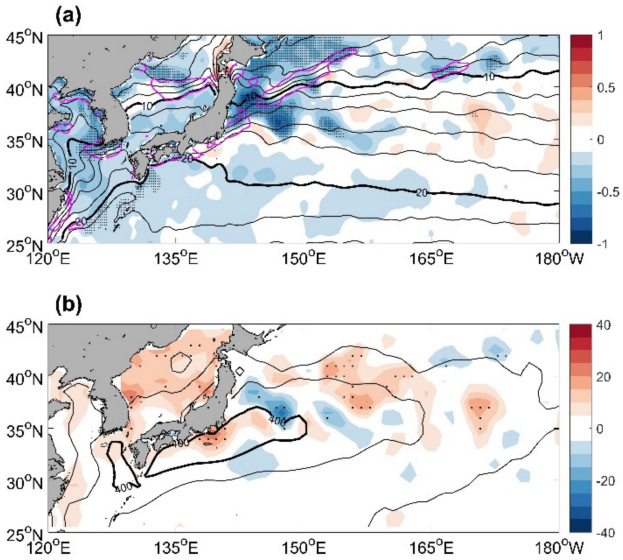


Figure 2. (**a**) The estimated SST response (shading, unit: °C) in DJF onto the KEI 2 months earlier and the climatological SST (contours at 2 °C intervals) in DJF. The SSTs at 10° and 20 °C are marked by the thick black contours. The magenta contours represent the climatological SST meridional gradient of -2.5×10^{-6} K m^{-1}. (**b**) The estimated THF response (shading, unit: Wm^{-2}) in DJF onto the KEI 2 months earlier and the climatological THF (contours at 100-Wm^{-2} intervals) in DJF. The THF at 400 Wm^{-2} is denoted by the thick black contours. A positive value of THF illustrates the upward transportation of THF from the ocean into the atmosphere. Stippling indicates the 90% confidence level.

3.2. EAT Responses to the KE Variability

Figure 3 presents the estimated atmospheric responses to the KE fluctuation. The colder 2 m air temperature anomaly of −2 K and the corresponding increase in snow cover of 15% extended from Mongolia to northeastern China, implying the potential impacts of the KE variability on EAWM (Figure 3a,b). In the middle troposphere, an anomalous cyclone center, coinciding with the climatological region of the EAT, was fully developed over East Asia (Figure 3c), accompanied with the accelerated (decelerated) westerly winds to the south (north) of 45° N in the upper troposphere (Figure 3d). These results all indicate that the EAT and associated EAWM intensified in the KE SPs, and the opposite for the USPs.

O'Reilly and Czaja [31] showed that when the KE jet was in its stable state, the 500-hPa geopotential height tended to decrease over East Asia in the 1993–2011 period, which is supportive of our results. Nevertheless, the study of Révelard et al. [32], which suggests a barotropic high response extending from East Asia to the central North Pacific in the stable phase of KE during 1979–2012, is contrary to the conclusions of us and O'Reilly and Czaja [31]. The further analysis shows that not only the local z_{500} response over East Asia but also the large-scale atmospheric circulation anomaly in the North Hemisphere bore opposite resemblances before and after 1992 (not shown). This prompts that there may also have existed a changing interdecadal relationship between the KE fluctuation and atmosphere during 1979–2018, which needs to be further investigated.

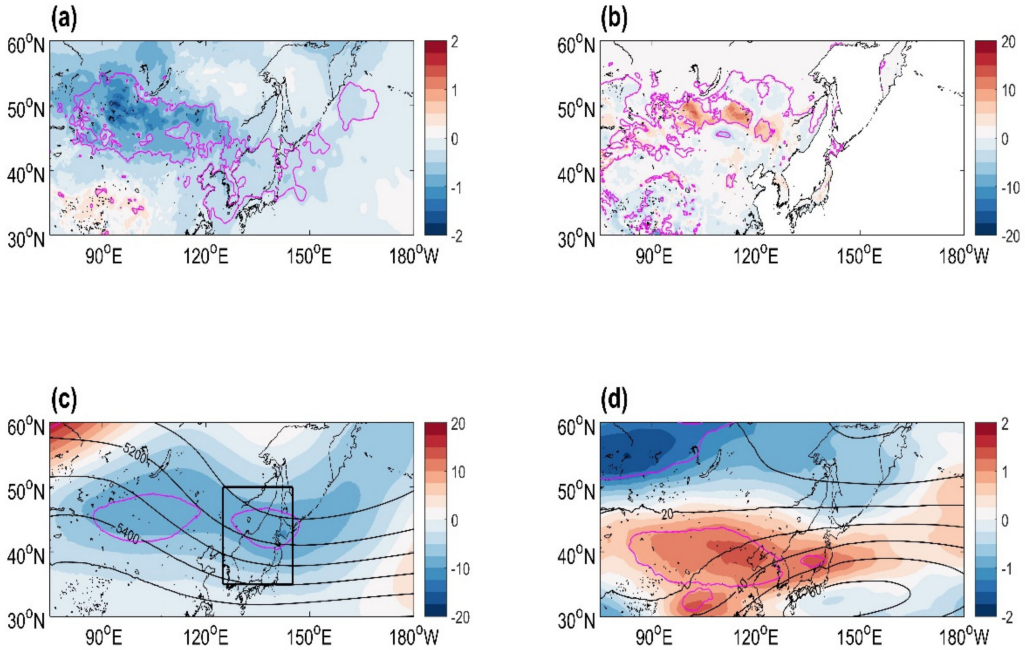


Figure 3. The estimated responses of (**a**) 2 m air temperature (shading, unit: K), (**b**) snow cover (shading, unit: %), (**c**) z_{500} (shading, unit: gpm), and (**d**) u_{300} (shading, unit: m s^{-1}) in DJF onto the KEI 2 months earlier. The thin black contours and thick black rectangle in (**c**) represent the climatological z_{500} in DJF and the area used for calculating the EATII, respectively. The climatological u_{300} in DJF is denoted by the black contours in (**d**). Magenta contours represent where the atmospheric anomalies are significant at the 90% confidence level.

The time series of the normalized KEI and EATII, depicted in Figure 4, show that the correlation coefficient between the KEI and EATII is −0.41, which is statistically significant at the 95% confidence level. After applying a lowpass filter to the EATII, the correlation coefficient reaches −0.66 at the 99% confidence level. This further proves that the EAT tends to be stronger in the presence of the stable KE, and vice versa for the unstable KE. Therefore, a question arises from this relationship: How does the KE variability influence the EAT intensity?

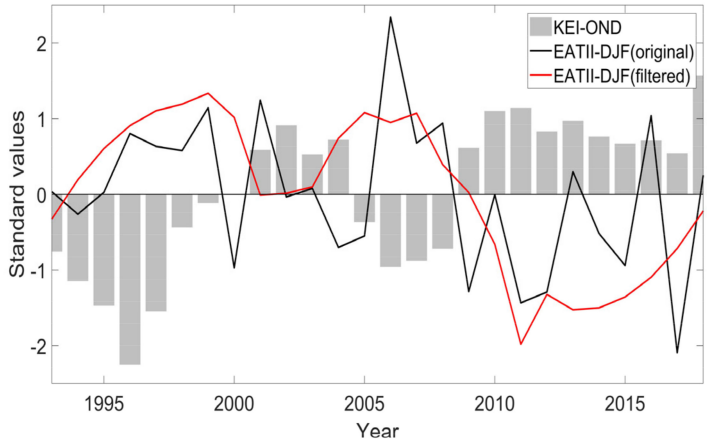


Figure 4. Normalized values of the KEI in OND (grey bar), EATII in DJF (black line), and lowpass EATII in DJF (red line). The lowpass EATII is calculated by applying a Savitzky–Golay filter with a window length of 11 years and a degree 2 polynomial to the EATII, to extract the EAT variation signal with the same frequency as the KE.

3.3. Possible Mechanisms

Some of the existing studies proposed that the SST anomalies play an important role in influencing the large-scale circulation, by forcing the atmospheric Rossby waves [32], eddy–mean flow interaction [29,31], and thermal winds [17,51]. Hence, in the following subsections, these three physical processes associated with the SST responses to the KE fluctuation will be discussed respectively.

3.3.1. Rossby Wave Activity

To understand how the KE-induced disturbance propagates, the anomalous RWS, WAF, and geopotential height are analyzed in Figures 5 and 6. Refs. [11,14] suggested that the Rossby waves driven by the pronounced positive SST anomalies in the mid-latitude North Atlantic can affect the EAT through the accumulation of the wave energy. In our study, as depicted in Figure 5, a RWS emerged in the middle and upper troposphere over the central and eastern parts of KE region, which may also arise from the underlying warm SST response. Conversely, forced by the cold SST anomalies near the Japan (Figure 2a), a noteworthy Rossby wave sink extended throughout the entire troposphere over East Asia. Figure 6b further shows that the KE excited the upward propagation of the WAF from the lower troposphere of the KE to the middle and upper troposphere and then posed a Rossby wave train propagating eastward along North America, the North Atlantic, northern Eurasia, and ultimately arriving the Rossby wave sink in East Asia (Figure 6). As a result, the Rossby wave activity played a critical role in decreasing the geopotential height (Figure 6a) and strengthening the EAT, leading to a deepening rate of approximately 0.075 gpm day^{-1}, which can explain 25% of the EAT amplification (Figure 7a).

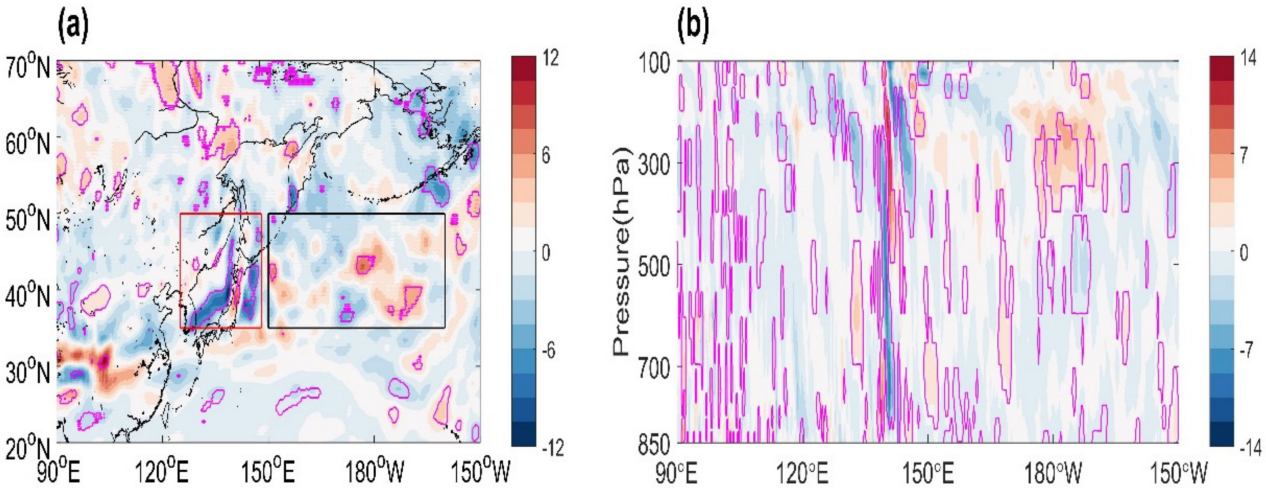


Figure 5. The estimated responses of RWS (shading, unit: 10^{-11} s^{-2}) (**a**) at the 300-hPa level and (**b**) along 35° N meridional average in DJF onto the KEI 2 months earlier. The red and black rectangular in (**a**) denote the Rossby wave sink and RWS related with the KE fluctuation, respectively. Magenta contours represent where the atmospheric anomalies are significant at the 90% confidence level.

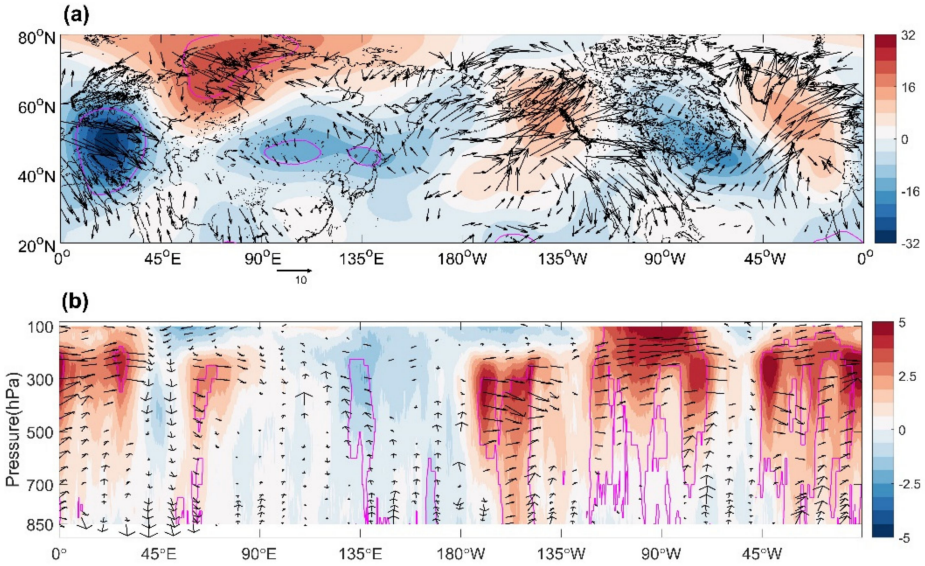


Figure 6. The estimated responses of (**a**) geopotential height (shading, unit: gpm) and horizontal WAF (vectors, unit: $m^2\ s^{-2}$) at the 300-hPa level and (**b**) zonal component of WAF (shading, unit: $m^2\ s^{-2}$) and WAF (vectors, unit: $m^2\ s^{-2}$ for horizontal component; -10^{-2} Pa $m\ s^{-2}$ for vertical component) along the 30°–80° N meridional average in DJF onto the KEI 2 months earlier. Magenta contours represent where the geopotential height and zonal component of WAF anomalies are significant at the 90% confidence level in (**a**,**b**) respectively. Only the WAF passing the 90% confidence level is plotted.

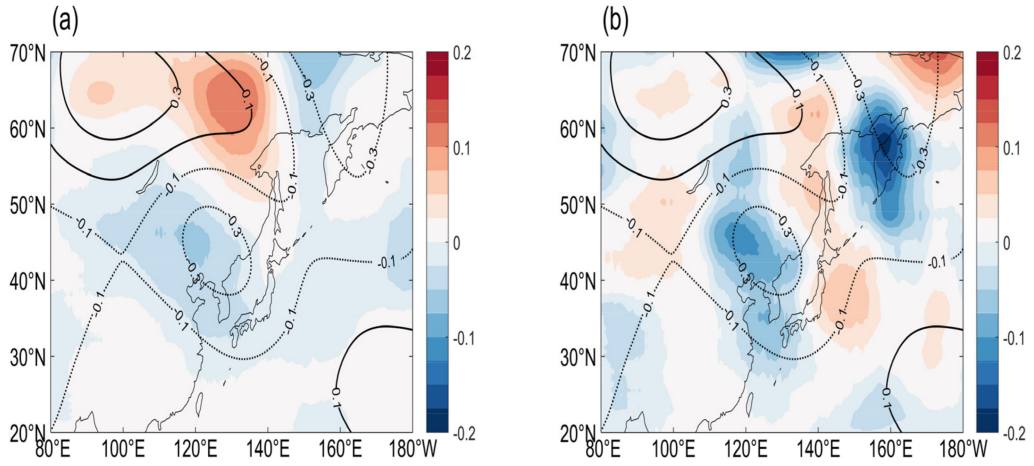


Figure 7. (**a**) The estimated response of Rossby wave-induced 500-hPa geopotential height tendency (shading, unit: gpm day^{-1}) in DJF onto the KEI 2 months earlier, overlapped with the estimated response of 500-hPa geopotential height tendency (contours, unit: gpm day^{-1}). (**b**) is the same as (**a**), but for the transient eddy-induced 500-hPa geopotential height tendency. The data have been smoothed using a 10° × 10° spatial average for clearer visibility.

3.3.2. Eddy–Mean Flow Interaction

The previous analysis reveals that the Rossby waves favored the development of the cyclone anomaly east of Japan (Figures 6a and 7a), resulting in the corresponding acceleration of the westerly winds between 35° N and 45° N south of the anomalous cyclone (Figure 3d). Figure 8a is the EGR response in the lower troposphere. Forced by the increased westerly winds, the EGR was enhanced in its climatological maximum region along the KE, causing the corresponding intensifying of the local storm track, which extended northeastward from Japan to the central Pacific (Figure 8b). As a result, the transient eddies-induced feedback forcing led to 42% of the EAT amplification with a deepening rate of 0.125 gpm day^{-1} (Figure 7b). The role of enhanced transient eddy

activity in strengthening the EAT is consistent with Zhang et al. [52], who suggested that the pressure tends to be lower when there are more cyclones.

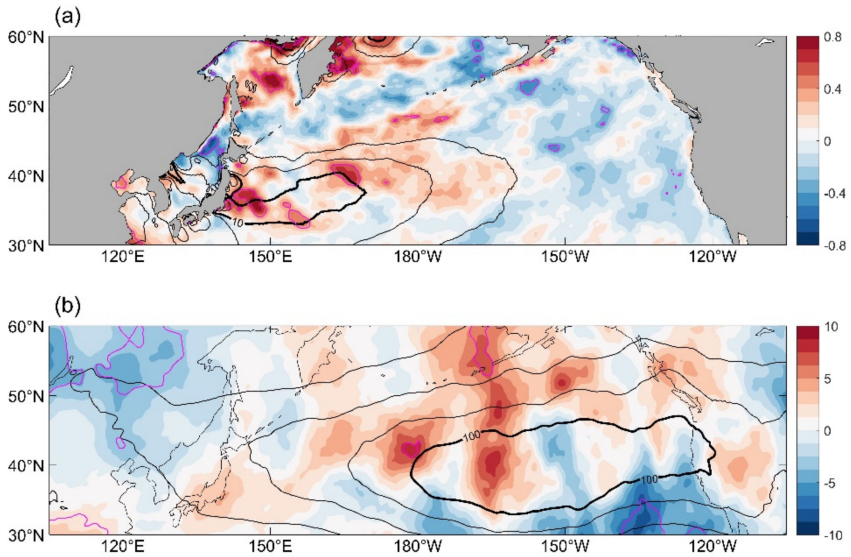


Figure 8. (**a**) The estimated EGR response (shading, unit: 10^{-6} s^{-1}) in DJF onto the KEI 2 months earlier and the climatological EGR (contours at 2×10^{-6} s^{-1} intervals) in DJF at the 850-hPa level. The EGR at 10^{-5} s^{-1} is marked by the thick black contours. The EGR over the continent is omitted because of the noisy impacts from the topography. (**b**) The estimated storm-track response (shading, unit: m^2 s^{-2}) in DJF onto the KEI 2 months earlier and the climatological storm track (contours at 20-m^2 s^{-2} intervals) in DJF at the 300-hPa level. The storm track at 100 m^2 s^{-2} is denoted by the thick black contours. Magenta contours represent where the atmospheric anomalies are significant at the 90% confidence level.

Refs. [53,54] found that the Pacific storm-track activity could largely impact the North Atlantic storm track via the link between synoptic wave-breaking events in the eastern Pacific and the Atlantic. In our results, when the KE was in the stable state, the storm track was significantly subdued over the midlatitude of North Atlantic Ocean (not shown), which may be driven by the disturbances of the North Pacific storm track and Rossby wave-induced baroclinicity weakness. The underlying mechanisms are not discussed here and need to be further investigated.

3.3.3. Thermal Winds

In addition to being able to impact the atmospheric circulation through the Rossby waves and transient eddies, the SST anomaly in the KE region can also modify the basic atmospheric flow via direct thermal forcing, as depicted by the thermal wind theory. The SST decrease of 0.5 K around 37° N cools the overlying atmosphere through suppressing THF by 10 W m^{-2} (Figure 9c), leading to the atmospheric responses titling northward as height increases, with the enhanced (weakened) meridional temperature gradient south (north) of 42° N on the 500-hPa level (Figure 9a). According to the thermal wind theory, the 500-hPa westerly winds south (north) of 42° N will be accelerated (decelerated), resulting in a significant anomalous cyclone over East Asia, which corresponds to a stronger EAT (Figure 9b). The similar physical process through which the SST anomaly in the northwestern Pacific influences the EAT is also addressed in [17,51], highlighting the importance of thermal wind process in SST modulating the EAT.

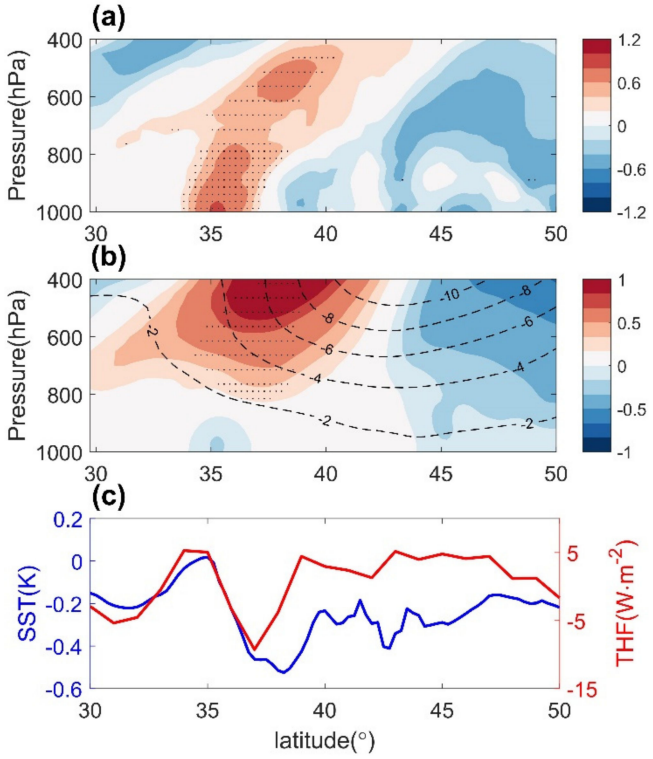


Figure 9. The estimated responses of (**a**) meridional temperature gradient (shading, unit: 10^{-6} Km^{-1}), (**b**) zonal winds (shading, unit: ms^{-1}), geopotential height (contour, unit: gpm), (**c**) SST (blue line, unit: K, left ordinate) and THF (red line, unit: Wm^{-2}, right ordinate) averaged between 140° E and 150° E. Stippling indicates the 90% confidence level. The meridional temperature gradient is multiplied by −1. A positive value indicates the meridional temperature gradient is enhanced.

3.4. The Effects of KE Fluctuation on the East Asian Winter Climate

Due to the stronger EAT in the SPs, cold horizontal heat transport is found over the rear of the EAT, while there is warm horizontal heat transport to the front of the EAT (Figure 10b). On the contrary, the enhanced descending motion related to the deepened EAT and larger THF warms up the air to the west of the EAT, whereas the air temperature is cooled down by the intensified ascending motion and suppressed THF to the east of the EAT (Figures 2b and 10c,d). As a result, though the horizontal heat transport is offset by the vertical transport and diabatic heating to some extent over the region from Lake Baikal to the Sea of Japan, it decreases the air temperature and thus leads to a colder winter climate. Meanwhile, the KE fluctuation has little impact on the air temperature to the front of the EAT, because the horizontal transport-caused warming trend is basically equal to the cooling trend generated by the vertical transport and diabatic heating (Figures 3a and 10a).

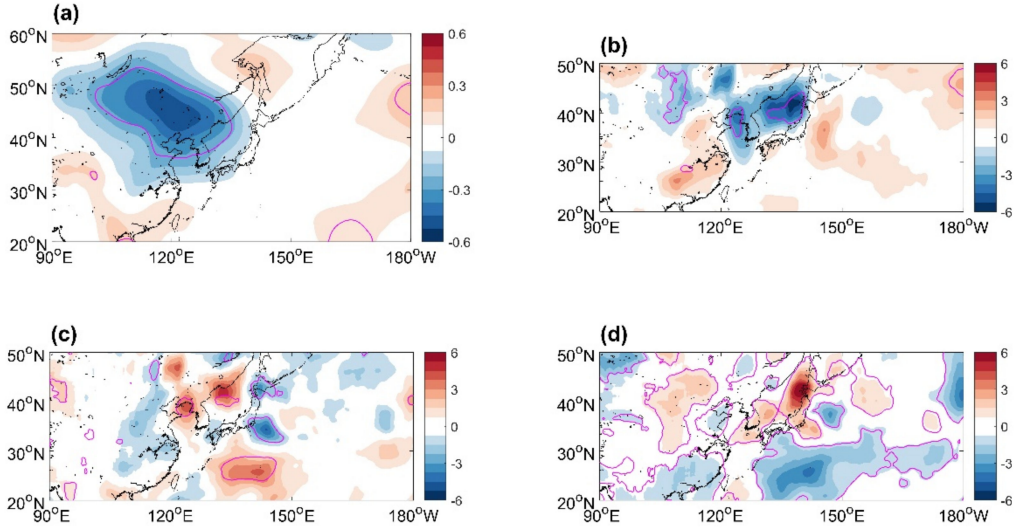


Figure 10. The estimated responses of (**a**) local air-temperature change (shading, unit: 10^{-6} Ks^{-1}), (**b**) horizontal heat transport (shading, unit: 10^{-6} Ks^{-1}), (**c**) vertical heat transport (shading, unit: 10^{-6} Ks^{-1}), and (**d**) diabatic heating (shading, unit: 10^{-6} Ks^{-1}) at the 850-hPa level in DJF onto the KEI 2 months earlier. The data have been smoothed using a $10^{\circ} \times 10^{\circ}$ spatial average for cleaner visibility. Stippling indicates the 90% confidence level.

4. Conclusions and Discussion

This study explores the impacts of the KE fluctuation on the EAT during the boreal winter and the underlying mechanisms by using the lag regression approach. We follow a KEI of [37], using the satellite SSHA data, to identify the dynamical state of the KE. In the positive phase of the index, the KE was stable with a stronger SST front, accompanied with the SST cooling (warming) and related suppressed (enhanced) THF in the western (eastern) part of the KE, implying the potential influences of KE variability on the overlying atmosphere through the sea–air interactions. The reverse holds when the index is negative.

It was found that in the KE SPs, the EAT is deeper than usual between December and February, with a stronger EAWM and an anomalous cyclonic circulation in the middle and upper troposphere over East Asia. As a result, the enhanced EAT drops the temperature by 2 K and increases the snow cover by 15% over Mongolia and northeastern China via intensifying cold horizontal heat transport.

The significant roles played by the atmospheric Rossby waves, transient eddies, and thermal winds are revealed. First, the SST warming in the eastern part of the KE acts as the RWS and excites the upward Rossby waves to the middle and upper troposphere. A Rossby wave train propagates across the North America, North Atlantic, and northern Eurasia to the EAT region. This leads to the Rossby wave convergence over East Asia and thus contributes to 25% magnitude of the EAT deepening. Second, the stable KE-induced Rossby waves facilitate the low-level baroclinicity, enhancing the storm track in the midlatitudes of the North Pacific and consequently leading to another 42% magnitude of the EAT deepening through the transient eddy-induced feedback forcing. Third, based on the thermal wind theory, the strong SST cooling near the eastern coast of the Japan increases (decreases) the meridional temperature gradient, thus accelerating (decelerating) the westerly winds to the south (north) of 42° N, resulting in a cyclone anomaly over East Asia. In conclusion, the three physical processes jointly lead to the strengthening of the EAT. It should be noted that the feedback forcings from Rossby waves and transient eddies on the EAT amplification are basically comparable to [11], who suggested that both the Rossby waves and transient eddies can lead to 30% of the EAT's amplification, though they focused on the intraseasonal variations of the EAT.

Several previous studies have linked the EAT and associated EAWM variations with the large-scale atmospheric teleconnection patterns such as AO, NAO, and Asian-Pacific

oscillation [14,55,56], snow and ice covers such as the Eurasian snow cover and Arctic sea-ice area [15,57], and SST patterns such as the North Pacific SST variation and SST cooling in the KE region [17,51]. In order to validate that the EAT's variability is indeed derived from the KE fluctuation instead of the other climate indices mentioned above, we perform a correlation analysis (Table 1). The NAO, which is highly correlated with the KEI (r = 0.44, $p < 0.1$), is not significantly correlated with the EATI. There is no climate index covarying with both the KE and EAT. Thus, it can be concluded that the atmospheric mechanisms revealed in this study are driven by the KE variability but not other atmospheric features. To our knowledge, this study is the first to address the potential impacts of the KE variability on the EAT and the underlying physical processes. In addition, our study highlights that not only the thermal wind process but also the Rossby wave and transient eddy activities are important in the EAT responses to the interannual KE SST anomalies, which is different from [17,51], who merely reveal the role of thermal wind theory in the decadal SST anomalies influencing the EAT.

Table 1. Pearson correlation coefficients between KEI in OND/EATII in DJF and important indices in OND, including the Arctic Oscillation (AO), North Atlantic Oscillation (NAO), Asian-Pacific oscillation (APO) teleconnection pattern indices, Eurasian snow cover (60–140° E, 40–65° N), Arctic sea-ice area (30.5–149.5° E, 72.5–83.5° N), North Pacific SST (120–180° E, 26–40° N), and Kuroshio SST (120–150° E, 20–40° N). The asterisk indicates the coefficient passing the 90% confidence level. The AO, NAO, and APO indices are from the Physical Sciences Laboratory of National Oceanic and Atmospheric Administration (https://psl.noaa.gov/data/climateindices/list/, accessed on 2 February 2021).

	AO	NAO	APO	Eurasian Snow Cover	Arctic Sea Ice Area	North Pacific SST	Kuroshio SST
KEI	0.08	0.44 *	0.05	0.28	−0.12	−0.03	−0.18
EATI	−0.14	−0.07	0.14	−0.19	0.16	0.23	0.28

Note: * indicates the correlation coefficient passing the 90% confidence level.

However, some problems still remain to be solved in the future. Figure 6a shows strong geopotential height responses over the U.S. Northern Atlantic coast and Mediterranean basin, implying the KE fluctuation can exert far-reaching impacts on the trough systems further downstream via the Rossby wave activity. The specific relationship and associated physical mechanisms need further investigation. In addition, as one of the most vulnerable regions to global climate change, the warming rate of the KE is two to three times faster than the global mean surface ocean warming rate [58–60], promoting the question of whether the KE warming is important in our understanding of future EAT and associated EAWM system changes. All these problems need to be answered by means of diagnostic analysis and numerical simulations in the next work.

Author Contributions: Conceptualization, J.S. and Y.J.; methodology, J.S. and Y.J.; software, J.S.; validation, J.S., Y.J. and Y.W.; formal analysis, Y.J.; investigation, Y.J.; resources, J.S.; data curation, J.S.; writing—original draft preparation, Y.J.; writing—review and editing, J.S. and S.Z.; visualization, J.S. and Y.J.; supervision, S.Z.; project administration, S.Z.; funding acquisition, S.Z., B.W. and H.W. All authors have read and agreed to the published version of the manuscript.

Funding: This research was funded by the National Key Research and Development Program of China (NKPs, 2019YFC1510102 and 2021YFC3101605), and the National Natural Science Foundation of China (NFSC, 41876130, 41975024, and 41976025).

Institutional Review Board Statement: Not applicable.

Informed Consent Statement: Not applicable.

Data Availability Statement: The AVISO SSHA data were acquired from the Copernicus Marine Environment Monitoring Service (http://marine.copernicus.eu/ accessed on 13 January 2021). The surface heat flux data were acquired from the WHOI (ftp://ftp.whoi.edu/pub/science/oaflux/, accessed on 5 January 2021). We are grateful to the ECMWF for providing the ERA5 (https://www.ecmwf.int/, accessed on 19 January 2022).

Conflicts of Interest: The authors declare no conflict of interest.

References

1. Wang, L.; Chen, W.; Zhou, W.; Huang, R. Interannual variations of East Asian trough axis at 500 hPa and its association with the East Asian winter monsoon pathway. *J. Clim.* **2009**, *22*, 600–614. [CrossRef]
2. Zhang, Y.; Sperber, K.R.; Boyle, J.S. Climatology and interannual variation of the East Asian winter monsoon: Results from the 1979–95 NCEP/NCAR reanalysis. *Mon. Weather Rev.* **1997**, *125*, 2605–2619. [CrossRef]
3. Nakamura, H.; Miyasaka, T.; Kosaka, Y.; Takaya, K.; Honda, M. Northern Hemisphere extratropical tropospheric planetary waves and their low-frequency variability: Their vertical structure and interaction with transient eddies and surface thermal contrasts. In *Climate Dynamics: Why Does Climate Vary?* John Wiley & Sons, Inc.: Hoboken, NJ, USA, 2010; Volume 189, pp. 149–179. [CrossRef]
4. Smagorinsky, J. The dynamical influence of large-scale heat sources and sinks on the quasi-stationary mean motions of the atmosphere. *Q. J. R. Meteorol. Soc.* **1953**, *79*, 2–366. [CrossRef]
5. Nakamura, H.; Izumi, T.; Sampe, T. Interannual and decadal modulations recently observed in the Pacific storm track activity and East Asian winter monsoon. *J. Clim.* **2002**, *15*, 1855–1874. [CrossRef]
6. Ren, X.; Zhang, Y.; Xiang, Y. Connections between wintertime jet stream variability, oceanic surface heating, and transient eddy activity in the North Pacific. *J. Geophys. Res. Atmos.* **2008**, *113*, D21. [CrossRef]
7. Ren, X.; Yang, X.; Chu, C. Seasonal variations of the synoptic-scale transient eddy activity and polar front jet over East Asia. *J. Clim.* **2010**, *23*, 3222–3233. [CrossRef]
8. Wen, M.; Yang, S.; Kumar, A.; Zhang, P. An analysis of the large-scale climate anomalies associated with the snowstorms affecting China in January 2008. *Mon. Weather Rev.* **2009**, *137*, 1111–1131. [CrossRef]
9. Zhou, W.; Chan, J.C.; Chen, W.; Ling, J.; Pinto, J.G.; Shao, Y. Synoptic-scale controls of persistent low Zuotemperature and icy weather over southern China in January 2008. *Mon. Weather Rev.* **2009**, *137*, 3978–3991. [CrossRef]
10. Staff Members of the Section of Synoptic and Dynamic Meteorology, Institute of Geophysics and Meteorology, Academia Sinica, Peking. On the general circulation over Eastern Asia (II). *Tellus* **1958**, *10*, 58–75.
11. Song, L.; Wang, L.; Chen, W.; Zhang, Y. Intraseasonal variation of the strength of the East Asian trough and its climatic impacts in boreal winter. *J. Clim.* **2016**, *29*, 2557–2577. [CrossRef]
12. Gong, D.; Wang, S.; Zhu, J. East Asian winter monsoon and Arctic oscillation. *Geophys. Res. Lett.* **2001**, *28*, 2073–2076. [CrossRef]
13. Feng, G.; Zou, M.; Qiao, S.; Zhi, R.; Gong, Z. The changing relationship between the December North Atlantic Oscillation and the following February East Asian trough before and after the late 1980s. *Clim. Dyn.* **2018**, *51*, 4229–4242. [CrossRef]
14. Qiao, S.; Feng, G. Impact of the December North Atlantic oscillation on the following February East Asian trough. *J. Geophys. Res. Atmos.* **2016**, *121*, 10074–10088. [CrossRef]
15. Luo, X.; Wang, B. How autumn Eurasian snow anomalies affect east Asian winter monsoon: A numerical study. *Clim. Dyn.* **2019**, *52*, 69–82. [CrossRef]
16. Sun, C.; Yang, S.; Li, W.; Zhang, R.; Wu, R. Interannual variations of the dominant modes of East Asian winter monsoon and possible links to Arctic sea ice. *Clim. Dyn.* **2016**, *47*, 481–496. [CrossRef]
17. Sun, J.; Wu, S.; Ao, J. Role of the North Pacific sea surface temperature in the East Asian winter monsoon decadal variability. *Clim. Dyn.* **2016**, *46*, 3793–3805. [CrossRef]
18. Hao, X.; He, S.; Wang, H.; Han, T. Quantifying the contribution of anthropogenic influence to the East Asian winter monsoon in 1960–2012. *Atmos. Chem. Phys.* **2019**, *19*, 9903–9911. [CrossRef]
19. Miao, J.; Wang, T.; Wang, H.; Zhu, Y.; Sun, J. Interdecadal weakening of the East Asian winter monsoon in the mid-1980s: The roles of external forcings. *J. Clim.* **2018**, *31*, 8985–9000. [CrossRef]
20. Kelly, K.A.; Small, R.J.; Samelson, R.M.; Qiu, B.; Joyce, T.M.; Kwon, Y.O.; Cronin, M.F. Western boundary currents and frontal air–sea interaction: Gulf Stream and Kuroshio Extension. *J. Clim.* **2010**, *23*, 5644–5667. [CrossRef]
21. Kwon, Y.O.; Alexander, M.A.; Bond, N.A.; Frankignoul, C.; Nakamura, H.; Qiu, B.; Thompson, L.A. Role of the Gulf Stream and Kuroshio–Oyashio systems in large-scale atmosphere–ocean interaction: A review. *J. Clim.* **2010**, *23*, 3249–3281. [CrossRef]
22. Nonaka, M.; Xie, S.-P. Covariations of sea surface temperature and wind over the Kuroshio and its extension: Evidence for ocean-to-atmosphere feedback. *J. Clim.* **2003**, *16*, 1404–1413. [CrossRef]
23. Small, R.D.; deSzoeke, S.P.; Xie, S.-P.; O'neill, L.; Seo, H.; Song, Q.; Cornillon, P.; Spall, M.; Minobe, S. Air–sea interaction over ocean fronts and eddies. *Dyn. Atmos. Ocean.* **2008**, *45*, 274–319. [CrossRef]
24. Qiu, B.; Chen, S. Variability of the Kuroshio Extension jet, recirculation gyre, and mesoscale eddies on decadal time scales. *J. Phys. Oceanogr.* **2005**, *35*, 2090–2103. [CrossRef]

25. Jiang, Y.; Zhang, S.; Xie, S.-P.; Chen, Y.; Liu, H. Effects of a Cold Ocean Eddy on Local Atmospheric Boundary Layer Near the Kuroshio Extension: In Situ Observations and Model Experiments. *J. Geophys. Res. Atmos.* **2019**, *124*, 5779–5790. [CrossRef]
26. Ma, J.; Xu, H.; Dong, C.; Lin, P.; Liu, Y. Atmospheric responses to oceanic eddies in the Kuroshio Extension region. *J. Geophys. Res. Atmos.* **2015**, *120*, 6313–6330. [CrossRef]
27. Wang, Y.; Liu, W. Observational evidence of frontal-scale atmospheric responses to Kuroshio Extension variability. *J. Clim.* **2015**, *28*, 9459–9472. [CrossRef]
28. Wang, Q.; Zhang, S.; Xie, S.-P.; Norris, J.R.; Sun, J.; Jiang, Y. Observed Variations of the Atmospheric Boundary Layer and Stratocumulus over a Warm Eddy in the Kuroshio Extension. *Mon. Weather Rev.* **2019**, *147*, 1581–1591. [CrossRef]
29. Ma, X.; Chang, P.; Saravanan, R.; Montuoro, R.; Hsieh, J.S.; Wu, D.; Lin, X.; Wu, L. Distant influence of Kuroshio eddies on North Pacific weather patterns? *Sci. Rep.* **2015**, *5*, 17785. [CrossRef]
30. Ma, X.; Chang, P.; Saravanan, R.; Montuoro, R.; Nakamura, H.; Wu, D.; Lin, X.; Wu, L. Importance of resolving Kuroshio front and eddy influence in simulating the North Pacific storm track. *J. Clim.* **2017**, *30*, 1861–1880. [CrossRef]
31. O'Reilly, C.H.; Czaja, A. The response of the Pacific storm track and atmospheric circulation to Kuroshio Extension variability. *Q. J. R. Meteorol. Soc.* **2015**, *141*, 52–66. [CrossRef]
32. Révelard, A.; Frankignoul, C.; Sennéchael, N.; Kwon, Y.O.; Qiu, B. Influence of the decadal variability of the Kuroshio Extension on the atmospheric circulation in the cold season. *J. Clim.* **2016**, *29*, 2123–2144. [CrossRef]
33. Taguchi, B.; Nakamura, H.; Nonaka, M.; Komori, N.; Kuwano-Yoshida, A.; Takaya, K.; Goto, A. Seasonal Evolutions of Atmospheric Response to Decadal SST Anomalies in the North Pacific Subarctic Frontal Zone: Observations and a Coupled Model Simulation. *J. Clim.* **2012**, *25*, 111–139. [CrossRef]
34. Révelard, A.; Frankignoul, C.; Kwon, Y.O. A multivariate estimate of the cold season atmospheric response to North Pacific SST variability. *J. Clim.* **2018**, *31*, 2771–2796. [CrossRef]
35. Ducet, N.; Le Traon, P.Y.; Reverdin, G. Global high-resolution mapping of ocean circulation from TOPEX/Poseidon and ERS-1 and -2. *J. Geophys. Res. Ocean.* **2000**, *105*, 19477–19498. [CrossRef]
36. Yu, L.; Weller, R.A. Objectively analyzed air–sea heat fluxes for the global ice-free oceans (1981–2005). *Bull. Am. Meteorol. Soc.* **2007**, *88*, 527–540. [CrossRef]
37. Qiu, B.; Chen, S.; Schneider, N.; Taguchi, B. A coupled decadal prediction of the dynamic state of the Kuroshio Extension system. *J. Clim.* **2014**, *27*, 1751–1764. [CrossRef]
38. Sardeshmukh, P.D.; Hoskins, B.J. The generation of global rotational flow by steady idealized tropical divergence. *J. Atmos. Sci.* **1988**, *45*, 1228–1251. [CrossRef]
39. Takaya, K.; Nakamura, H. A formulation of a wave-activity flux for stationary Rossby waves on a zonally varying basic flow. *Geophys. Res. Lett.* **1997**, *24*, 2985–2988. [CrossRef]
40. Takaya, K.; Nakamura, H. A formulation of a phase-independent wave-activity flux for stationary and migratory quasigeostrophic eddies on a zonally varying basic flow. *J. Atmos. Sci.* **2001**, *58*, 608–627. [CrossRef]
41. Hoskins, B.J.; Valdes, P.J. On the existence of storm-tracks. *J. Atmos. Sci.* **1990**, *47*, 1854–1864. [CrossRef]
42. Sun, Z.; Zhang, J. Statistical characteristics of 40–60 day oscillation in extratropical area. In Proceedings of the Long-Term Weather Forecast; Ocean Press: Beijing, China, 1992; pp. 29–35.
43. Lau, N.C.; Nath, M.J. Model simulation and projection of European heat waves in present-day and future climates. *J. Clim.* **2014**, *27*, 3713–3730. [CrossRef]
44. Bretherton, C.S.; Widmann, M.; Dymnikov, V.P.; Wallace, J.M.; Bladé, I. The Effective Number of Spatial Degrees of Freedom of a Time-Varying Field. *J. Clim.* **1999**, *12*, 1990–2009. [CrossRef]
45. Ferreira, D.; Frankignoul, C. The transient atmospheric response to midlatitude SST anomalies. *J. Clim.* **2005**, *18*, 1049–1067. [CrossRef]
46. Ferreira, D.; Frankignoul, C. Transient atmospheric response to interactive SST anomalies. *J. Clim.* **2008**, *21*, 576–583. [CrossRef]
47. Frankignoul, C.; Czaja, A.; L'Heveder, B. Air–sea feedback in the North Atlantic and surface boundary conditions for ocean models. *J. Clim.* **1998**, *11*, 2310–2324. [CrossRef]
48. Liu, Z.; Wu, L. Atmospheric Response to North Pacific SST: The Role of Ocean–Atmosphere Coupling. *J. Clim.* **2004**, *17*, 1859–1882. [CrossRef]
49. Liu, Z.; Wen, N.; Liu, Y. On the assessment of nonlocal climate feedback. Part I: The generalized equilibrium feedback assessment. *J. Clim.* **2008**, *21*, 134–148. [CrossRef]
50. Frankignoul, C.; Sennéchael, N.; Kwon, Y.O.; Alexander, M.A. Influence of the meridional shifts of the Kuroshio and the Oyashio Extensions on the atmospheric circulation. *J. Clim.* **2011**, *24*, 762–777. [CrossRef]
51. Lei, T.; Li, S.; Luo, F.; Liu, N. Two dominant factors governing the decadal cooling anomalies in winter in East China during the global hiatus period. *Int. J. Climatol.* **2020**, *40*, 750–768. [CrossRef]
52. Zhang, M.; Perrie, W.; Long, Z. Springtime North Pacific Oscillation and summer sea ice in the Beaufort sea. *Clim. Dyn.* **2019**, *53*, 671–686. [CrossRef]
53. Chang, E.K. Are the Northern Hemisphere winter storm tracks significantly correlated? *J. Clim.* **2004**, *17*, 4230–4244. [CrossRef]
54. Drouard, M.; Rivière, G.; Arbogast, P. The North Atlantic Oscillation response to large-scale atmospheric anomalies in the northeastern Pacific. *J. Atmos. Sci.* **2013**, *70*, 2854–2874. [CrossRef]

55. Song, L.; Wu, R. Comparison of intraseasonal East Asian winter cold temperature anomalies in positive and negative phases of the Arctic Oscillation. *J. Geophys. Res. Atmos.* **2018**, *123*, 8518–8537. [CrossRef]
56. Zhou, B.; Xu, Y.; Shi, Y. Present and future connection of Asian-Pacific Oscillation to large-scale atmospheric circulations and East Asian rainfall: Results of CMIP5. *Clim. Dyn.* **2018**, *50*, 17–29. [CrossRef]
57. Zuo, J.; Ren, H.; Xue, B.; Li, W. Predictability of winter temperature in China from previous autumn Arctic sea ice. *Clim. Dyn.* **2016**, *47*, 2331–2343. [CrossRef]
58. Sakamoto, T.T.; Hasumi, H.; Ishii, M.; Emori, S.; Suzuki, T.; Nishimura, T.; Sumi, A. Responses of the Kuroshio and the Kuroshio Extension to global warming in a high-resolution climate model. *Geophys. Res. Lett.* **2005**, *32*. [CrossRef]
59. Wu, L.; Cai, W.; Zhang, L.; Nakamura, H.; Timmermann, A.; Joyce, T.; McPhaden, M.J.; Alexander, M.; Qiu, B.; Visbeck, M.; et al. Enhanced warming over the global subtropical western boundary currents. *Nat. Clim. Chang.* **2012**, *2*, 161–166. [CrossRef]
60. Zhang, X.; Wang, Q.; Mu, M. The impact of global warming on Kuroshio Extension and its southern recirculation using CMIP5 experiments with a high-resolution climate model MIROC4h. *Theor. Appl. Climatol.* **2017**, *127*, 815–827. [CrossRef]